ACS Catalysis

Research Article

pubs.acs.org/acscatalysis

Selective Catalytic Reduction of NO_x with Ammonia over Soot

M. Mehring, M. Elsener, and O. Kröcher*

Paul Scherrer Institute, 5232 Villigen PSI, Switzerland

ABSTRACT: The selective catalytic reduction (SCR) of nitrogen oxides (NO_x) in the presence of NH_3 was investigated on Printex U and three diesel soot samples in the temperature range between 200 and 350 °C. In the presence of NO + NO_2, a stoichiometry similar to that of the *fast SCR* reaction was observed, whereas in the absence of NO, the stoichiometry shifted to values typical of the *NO_2 SCR* reaction. In the presence of only NO, no NO_x reduction was observed. Carbon oxidation and SCR reaction minimally influenced each other. On the basis of these experimental results, a mechanism for NO_x reduction over diesel soot was developed. The first step in the reaction is the disproportionation of NO_2, which is followed by the formation of ammonium nitrates and nitrites. The nitrites decompose directly into N_2 and H_2O, whereas the nitrates have to be reduced to nitrites either by NO or in its absence by NH_3, which also leads to the formation of N_2 and H_2O. The observed byproducts indicated that the acidity and the amount of surface functional groups for NH_3 are important preconditions for the occurrence of the SCR reaction over soot.

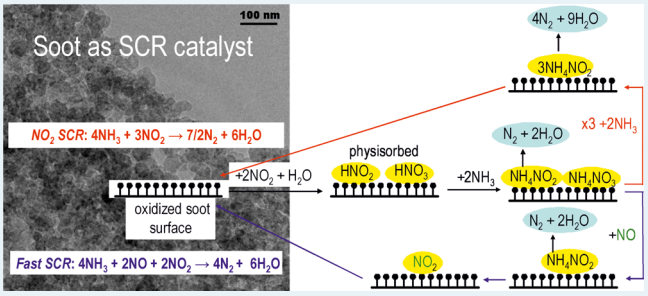

KEYWORDS: *selective catalytic reduction, NO_x reduction, soot oxidation, diesel soot, fast SCR, NO_2 SCR*

1. INTRODUCTION

Today's research in the field of exhaust gas after-treatment is mainly driven by the tightening of the legal emission limits for soot particulates and nitrogen oxides in the exhaust gas of diesel engines. Soot particulate emissions have been successfully reduced by the application of diesel particulate filters (DPF),[1,2] where the soot is accumulated and oxidized to CO_2 with O_2 or O_2–NO_2 mixtures as oxidants.[3]

One of the most efficient technologies for the reduction of NO_x emissions in lean exhaust gases is the selective catalytic reduction (SCR) with NH_3[4−6] over catalysts based on V_2O_5/WO_3–TiO_2 or Cu- and Fe-zeolites.[7−9] In this process, urea, which is used as a harmless NH_3 precursor, is dosed to the hot exhaust gas, where it decomposes in a two-step reaction to ammonia with isocyanic acid as an intermediate:

$$H_2N{-}C(O){-}NH_2 \rightarrow HNCO + NH_3 \quad (1)$$

$$HNCO + H_2O \rightarrow CO_2 + NH_3 \quad (2)$$

Three SCR overall reaction equations describe the stoichiometries observed under different conditions and with different catalysts:[4,10]

standard SCR

$$4NH_3 + 4NO + O_2 \xrightarrow{Cat} 4N_2 + 6H_2O \quad (3)$$

fast SCR

$$4NH_3 + 2NO + 2NO_2 \xrightarrow{Cat} 4N_2 + 6H_2O \quad (4)$$

NO_2 SCR

$$4NH_3 + 3NO_2 \xrightarrow{Cat} 7/2N_2 + 6H_2O \quad (5)$$

Thus far, it has been possible to achieve the legal emission limits through the application of either a SCR system or a DPF system with the appropriate adaptation of the combustion conditions. However, the implementation of more restrictive limits in the future necessitates the application of both a particulate filter and an SCR system in the same vehicle. Although such a combination satisfies the desired emission limits, this combination results in a disadvantageous weight and cost increase. Therefore, ideas for the combination of both functions in one after-treatment device are encouraged. According to this concept, a DPF and SCR catalyst could be placed within the same housing, or the filter structures could be coated with SCR-active materials. This arrangement would consequently lead to the parallel presence of NO_x, reducing agent, and diesel soot in one reaction compartment, where they may react with each other. This combination comprises known reactions, which have not been relevant until now because the reactants have not previously been in contact in emission systems, and likely also new reactions that have not been previously considered. Studies of the chemistry in combined DPF-SCR systems are required for a proper design and before such systems can be introduced into the market.

Received: March 20, 2012
Revised: May 29, 2012
Published: June 1, 2012

   dx.doi.org/10.1021/cs300184q | *ACS Catal.* 2012, 2, 1507−1518

In fact, similar reaction systems have been described in the literature. In the 1980s, researchers found that NO in the exhaust gases of industrial processes could be reduced over highly activated carbons in the presence of NH_3.[11−14] The oxidation of NO to NO_2 was recognized as a prerequisite step for the occurrence of the SCR reaction.[15−17] Although NO oxidation appears to proceed relatively efficiently over activated carbons at low temperatures, which is discernible from their higher SCR activity in this temperature region compared to typical metal-oxide-based catalysts, the general SCR activity of carbon is still relatively low. Therefore, the applied space velocities were most often less than 2000 h^{-1}.[15,18−20]

These previous results have raised the question of whether soot might also act as a catalyst for NO_x reduction in combined DPF−SCR systems even though space velocities are more than ten times higher in mobile applications. Therefore, a laboratory study was performed to investigate the influence of typical diesel exhaust gas components, that is, NO_2, NO, NH_3, and H_2SO_4, on the SCR activity of diesel and model soot.[21] Furthermore, the relationship between soot oxidation and SCR process on soot, which occur in parallel, was examined.

2. EXPERIMENTAL SECTION

2.1. Samples and Their Characterization. Four different powdered soot samples were used in our study: commercially available Printex U from Evonik (Germany), a soot of a diesel engine that satisfies Euro V emission limits, a soot of a diesel engine that satisfies Euro 0 limits, and a soot mixture obtained from several diesel engine test benches (labeled as mixed soot).

The largest number of experiments was performed with Printex U because it was available in sufficient amounts, and it is a well-characterized model substance for diesel soot.[22−24] The diesel soot samples were available only in small amounts, and the number of experiments was therefore limited; the conducted experiments were mainly used to confirm the transferability of the Printex U results to real systems.

The composition of the four soot samples was analyzed on a TG-FTIR system (thermogravimetric analyzer TGA/DSC1 from Mettler-Toledo combined with an Antaris IGS Fourier-transform infrared spectrometer from ThermoScientific) that was specially equipped for the characterization of soot samples.[25] This system allowed the quantification of the elemental and organic carbon (EC and OC) contents plus the amounts of oxygen, hydrogen, organic nitrogen, organic sulfur and sulfuric acid (detected as SO_2), and water as well as the ash content.[25,26] In addition, the Brunauer−Emmett−Teller (BET) surface areas of the samples were measured using nitrogen physisorption on a Quantachrom Autosorb 1-c instrument, and the ash was characterized using ICP-OES measurements on a Varian VISTA PRO AX instrument.

2.2. Activity Measurements. The SCR activity of soot was primarily investigated in a heated tubular quartz reactor with a length of 650 mm and an inner diameter of 49 mm. The flowchart of the experimental setup is shown Figure 1.

After the feed gases entered the reactor, they were temperature-controlled in the preheating zone (first heating zone), which was filled with ceramic beads for effective heat transfer. After passing through the frit, the gases entered the reaction zone (second heating zone), where the sample holder was placed. The last heating zone (third heating zone) controlled the reactor outlet downstream of the sample, where approximately 10−15% of the product gas flow was continuously extracted for gas analysis.

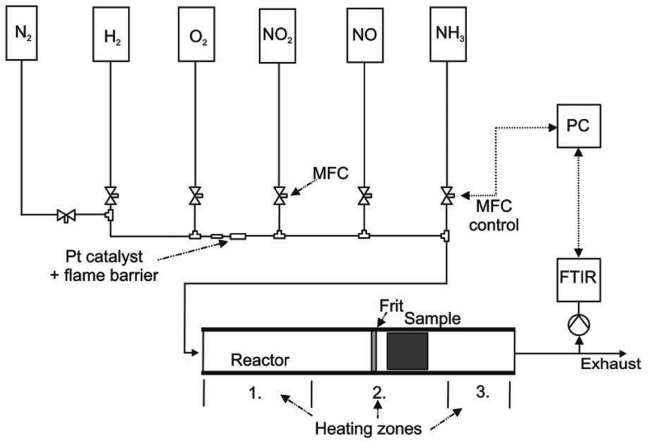

Figure 1. Flowchart of the experimental setup. The dotted lines represent the communication connections of the FTIR spectrometer and the MFCs with the PC.

The soot samples were brought into the reactor coated on cuboid cordierite monoliths ($L \times H \times W$ = 22 mm ×26.5 mm ×26.5 mm) with a cell density of 400 cpsi. They were loaded with approximately 60 mg of soot by dip-coating of the monoliths with dispersions of the soot samples in isopropyl alcohol. The solvent was removed with an air blower for 2 min, and the samples were subsequently dried at 85 °C in a cabinet dryer for 4 h. The blank and loaded dry monoliths were weighed to allow an estimation of the load. The gas hourly space velocity (GHSV), calculated from the quotient of the total gas flow and the volume of the cordierite monoliths, was 35,000 h^{-1} unless otherwise noted. To investigate the influence of sulfuric acid (H_2SO_4) on the soot activity, some of the soot-loaded monoliths were impregnated with 5 mg of H_2SO_4 in a second step.

The reactive gases were provided by a gas mixing unit that consisted of six mass flow controllers (Brooks 5850S). The total flow was 550 L/min at STP depending on the desired space velocity. The base feed gas consisted of 10% oxygen and 5% water with nitrogen as the balance. Water was generated by controlled hydrogen oxidation over a Pt catalyst. NO_2, NH_3, and NO were added to the base feed gas in varying concentrations.

The gas flows were analyzed quantitatively using a Nicolet Nexus FTIR spectrometer with a gas-measuring cell with a path length of 2 m and a liquid-nitrogen-cooled mercury cadmium telluride MCT detector. The spectrometer was calibrated for CO_2, CO, NO, NO_2, NH_3, N_2O, HCN, HNCO, HNO_3, HONO, SO_2, and H_2SO_4. All tubes downstream of the gas mixing unit as well as the FTIR cell were heated to 180 °C to avoid condensation. Each spectrum was the average of 8 scans at a resolution of 0.5 cm^{-1}. HNO_3 and, to a greater extent, HONO showed cross-sensitivities to NH_3 in the FTIR spectra, which could not be removed by the QuantPad calibration software. Therefore, the results for HNO_3 had to be analyzed carefully, and in the case of HONO, spectral analysis was only possible in the absence of NH_3 because the HONO signal showed an additional baseline shift.

The measurements were performed isothermally with soot samples treated for 25 min with 10% O_2 + 5% H_2O + 250 ppm NO_2 + 250 ppm NH_3 in the feed gas for activation. After the activation, the NH_3, NO, and NO_2 concentrations were varied consecutively in concentration series (series 1−3) according to

dx.doi.org/10.1021/cs300184q | ACS Catal. 2012, 2, 1507−1518

Table 1 while each feed mixture was maintained for 5 min. NO without NO_2 was not taken into consideration in the series

Table 1. Variation of the NO_2, NO, and NH_3 Concentrations for the Isothermal Investigation of the SCR Effect on Soot[a]

	series	NO_2 [ppm]	NH_3 [ppm]	NO [ppm]
NH_3 variation	1	250	100, 250, 500	0
NO variation	2	250	250	100, 250, 500
NO_2 variation	3	100, 250, 500	250	0

[a]Between each series, the sample was flushed with 10% O_2 + 5% H_2O with nitrogen as a balance for 10 min.

experiments because no SCR activity was observed in the absence of NO_2 during preliminary experiments. One soot-coated monolith was used for each investigated temperature.

Series 1−3 were repeated three to five times. When the carbon consumption on the monoliths exceeded 50−60%, the measurements were terminated to exclude influences from the limitation of the amount of available soot. The samples were subsequently heated to 700 °C with 10% O_2 in the feed gas to estimate the total carbon amount. For comparison of the different experiments, the series that showed the maximum NO_x reduction values were used. Loss of soot by the gas flow could be excluded as the average soot recovery in the FTIR analysis was 100% (± 5%) which is within the measurement error of the experiments.

For the investigation of the SCR reaction with 250 ppm NO and 250 ppm NH_3 without NO_2 in the presence of 5% H_2O and 10% O_2, we performed a temperature-programmed reaction experiment between 200 and 450 °C at 3000 h^{-1}. To reach this GHSV, the total flow was reduced to 275 L/h at STP, and a cylindrical monolith (L = 56 mm; Ø = 45 mm) was used.

In addition to the activity measurements in the tubular reactor, DRIFTS (diffuse reflectance infrared Fourier-transform spectroscopy) measurements on Printex U were also performed to investigate the functional groups formed by the adsorption of NO_2 and NH_3 in the presence of H_2O and O_2. The measurements were performed using a Thermo Scientific Nexus 600 FTIR spectrometer and a Thermo Scientific DRIFTS cell. The cell was heatable and was equipped with ZnSe windows. For the background collection, the feed gas always contained 10% O_2 + 5% H_2O in nitrogen. Then, 1000 ppm NO_2 and 1000 ppm NH_3 were added to the feed gas for 20 min. The system was subsequently purged for 20 min with 10% O_2 + 5% H_2O in nitrogen to allow a final spectrum that contained only absorption bands of the chemisorbed species to be collected.

2.3. Data Analysis. *2.3.1. NO_x Reduction.* The NO_x reduction describes the activity of the soot samples to reduce NO_x in the feed gas during the SCR reaction. We used the amount of reduced NO_x either as a relative quantity in [%]:

$$NO_x reduction\ [\%] = \frac{NO_{x,\mathrm{in}} - NO_{x,\mathrm{out}}}{NO_{x,\mathrm{in}}} \cdot 100 \tag{6}$$

or as an absolute quantity in [ppm]:

$$NO_x reduction\ [\mathrm{ppm}] = NO_{x,\mathrm{in}} - NO_{x,\mathrm{out}} \tag{7}$$

where $NO_{x,\mathrm{in}}$ represents the NO_x inlet concentration in the feed gas in [ppm] and $NO_{x,\mathrm{out}}$ represents the measured NO_x outlet concentration in [ppm].

2.3.2. Stoichiometric Ratio. During the SCR reaction, NH_3 and NO_x react with each other. On the basis of the converted amounts of NH_3 and NO_x estimated from their concentration differences in the feed gas inlet and outlet, an experimental stoichiometric ratio A of the SCR reaction was defined as follows:

$$A = \frac{NH_{3,\mathrm{in}} - NH_{3,\mathrm{out}}}{NO_{x,\mathrm{in}} - NO_{x,\mathrm{out}}} \tag{8}$$

where $NH_{3,\mathrm{in}}$ represents the NH_3 inlet concentration in the feed gas in [ppm] and $NH_{3,\mathrm{out}}$ is the sum of the measured NH_3, HCN, and HNCO outlet concentrations, as HCN and HNCO were formed almost exclusively from the reaction of NH_3 with surface species of the soot sample.

2.3.3. Carbon Oxidation Rate. The carbon oxidation rate (C-oxidation rate) was used to quantify the amount of carbon that is released from a soot sample by decomposition of the surface functional groups formed at time t. The C-oxidation rate is defined as the ratio of the carbon amount in the gas phase at time t ($c_{\mathrm{gas},t}$) in [μg] calculated from the CO, CO_2, HNCO, and HCN concentration in the gas phase detected in the FTIR spectrum at time t, and the amount of carbon at time t ($c_{\mathrm{solid},t}$) in [mg] remaining in the solid phase correlated to the period of time needed for the collection of a FTIR spectrum t_{collect} in [s]:

$$\text{C-oxidation rate}\left[\frac{\mu g}{mg \cdot s}\right] = \frac{c_{\mathrm{gas},t}}{c_{\mathrm{solid},t}} \cdot \frac{1}{t_{\mathrm{collect}}} \tag{9}$$

The parameter $c_{\mathrm{solid},t}$ was calculated from the total amount of carbon at the beginning of the measurements $c_{\mathrm{solid},0}$ minus the sum of carbon desorbed up to time t. This method of calculating the C-oxidation rate is similar to a normalization of the data, which allows the comparison of the results of different reactive gases and samples of different sizes.

3. RESULTS AND DISCUSSION

3.1. Sample Characterization. Figure 2 shows the results of the composition analysis of the four soot samples. The diagram depicts the sum hydrogen, sulfate, water, nitrogen, oxygen, OC, and EC calculated back from measured gas phase concentrations plus the ash content compared to the initial weight. The relative error of this comparison was ±4.5% of the

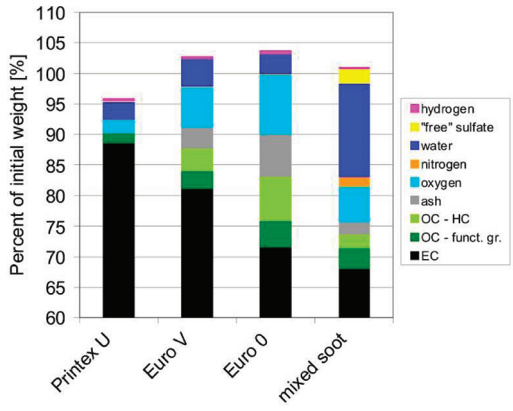

Figure 2. Results of the composition analysis of Printex U, Euro V soot, Euro 0 soot, and the mixed soot based on TG-FTIR measurements. The range from 0 to 60% consisted of EC.

dx.doi.org/10.1021/cs300184q | ACS Catal. 2012, 2, 1507−1518

initial weight for the components measured in the gas phase and ±0.6% of the initial weight for the ash content. Printex U exhibited the largest EC content and the smallest oxygen, hydrogen and water contents among the samples. The EC content of the samples decreased in the following order: Euro V > Euro 0 > mixed soot sample. The Euro 0 sample exhibited the largest ash and OC contents. In contrast to Printex U, the three diesel soot samples contained a fraction of nitrogen, which was evolved mainly as NH_3 in the case of the mixed soot and as NO from the Euro V and Euro 0 samples. The water contents of the samples were relatively low, except for the mixed soot. Printex U and the mixed soot sample contained a fraction of H_2SO_4.

The ash analysis of the diesel soot samples by ICP-OES showed that their ash consisted of a large number of metallic and nonmetallic ions. Printex U did not contain metals at concentrations above the detection limits of the ICP-OES analysis. Table 2 summarizes the metals with the highest concentrations in the ash of the Euro V, Euro 0, and mixed soot samples.

Table 2. Amounts of the Most Important Metals Detected in the Euro 0, Euro V, and Mixed Soot Samples

	Euro 0 [wt %]	mixed soot [wt %]	Euro V [wt %]
Ca	1.52	0.42	0.92
Fe	0.96	0.68	0.99
K	0.02	0.02	0.02
Mg	0.05	0.08	0.04
Na	0.34	0.26	0.03
Zn	0.46	0.24	0.08

The measured BET surface areas of the samples did not differ significantly and were small compared with those of activated carbons. The BET surface areas of Printex U, Euro V, Euro 0, and the mixed soot samples were 103, 110, 132, and 145 m^2/g, respectively.

3.2. SCR Activity of Printex U in the Presence of NO and NH_3. NO has been reported in the literature to be reduced to nitrogen in the presence of O_2, H_2O and NH_3 at space velocities of approximately 2000 h^{-1}, and the oxidation of NO to NO_2 by oxygen has been reported to be the key step in this process.[15−17] However, in a preliminary TPR experiment with Printex U under the same reaction conditions reported in the literature, we did not observe any SCR activity. In Figure 3, the NO_x reduction, the NH_3 conversion U_{NH3}, the NO, NO_2, NH_3 concentrations, and the sum of the nitrogen components in the presence of NO are plotted between 200 and 450 °C at a GHSV of 3000 h^{-1}.

The NH_3 concentration remained constant up to 280 °C. At higher temperatures, it decreased together with the sum of the nitrogen components, whereas the NO concentration slightly increased, which led to a negative NO_x reduction. However, the NH_3 conversion increased faster than the NO concentration. NO_2 was not observed during the course of the measurement. From these results, Printex U is concluded not to be active for NO oxidation and NO_x reduction under these conditions; it is, however, able to selectively oxidize NH_3 to nitrogen,[27] as confirmed by a blank experiment with a feed gas that contained only 10% O_2 + 5% H_2O + 250 ppm NH_3 with nitrogen as the balance. Furthermore, a comparison of the nitrogen balance of the blank experiment with the experiment in the presence of soot and soot oxidation experiments in the presence of NO showed that NO did not undergo any other reactions with the soot surface in combination with H_2O and/or O_2.

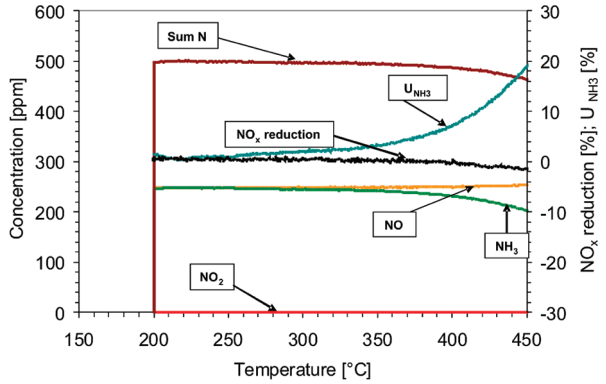

Figure 3. NO_x reduction, NH_3 conversion, and the concentrations of NO, NO_2, NO_x, and NH_3 on Printex U at a space velocity of 3000 h^{-1} during a TPR investigation with 250 ppm NO + 250 ppm NH_3 from 200 to 450 °C. The sum of the nitrogen-containing components is also shown.

3.3. SCR Activity of Printex U in the Presence of NO_2, NO, and NH_3. Although no SCR activity was observed in the TPR experiment with NO and NH_3 in the feed gas, a further preliminary experiment showed that in the presence of NO_2, Printex U was SCR-active. Therefore, NO_2 was always added in the main experiments for the investigation of the NO_x reduction over soot.

Figure 4 shows the NO_x reduction in [ppm] over Printex U at temperatures between 200 and 350 °C for different concentrations of NO_2, NO, and NH_3, as detailed in Table 1. The NO_x reduction was plotted in absolute values according to 7 since plotting the relative NO_x reduction in [%] according to 6 would not directly show the significant increase of the NO_x reduction in the presence of NO. A comparison of 6 and 7 discloses that the trends illustrated in Figure 4 would be inverted when plotting relative NO_x reduction rates due to the different NO_x inlet concentrations; however, the absolute values actually increased. Higher temperatures were not considered in the figures because the rate of carbon oxidation and the rate of NH_3 oxidation to N_2 became too large for

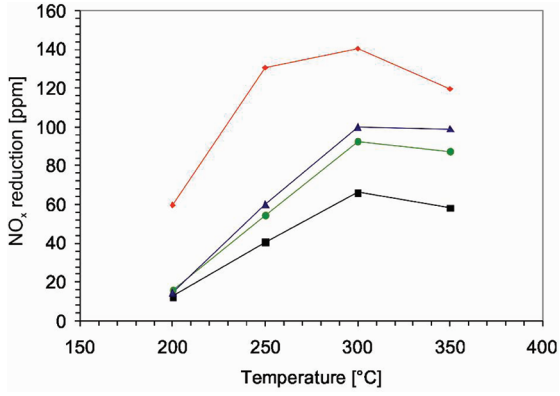

Figure 4. Dependence of the NO_x reduction over Printex U on the NO_2, NO and NH_3 concentrations between 200 and 350 °C calculated according to 7. black filled squares, 250 ppm NO_2 + 250 ppm NH_3; green filled circles, 250 ppm NO_2 + 500 ppm NH_3; blue filled triangles, 500 ppm NO_2 + 250 ppm NH_3; red filled diamonds, 250 ppm NO_2 + 250 ppm NH_3 + 250 ppm NO.

dx.doi.org/10.1021/cs300184q | ACS Catal. 2012, 2, 1507−1518

reproducible NO_x reduction rates to be measured. However, at temperatures below 200 °C, the NO_x reduction activity was too small to be analyzed reliably.

In the presence of 250 ppm NO_2 + 250 ppm NH_3, 12 ppm NO_x were reduced at 200 °C, which increased to the maximum NO_x reduction of 66 ppm at 300 °C corresponding to a relative NO_x reduction of 25%. At temperatures above 300 °C, the NO_x reduction was slightly reduced because of the occurrence of NH_3 oxidation.

When the NH_3 concentration was increased to 500 ppm the maximum NO_x reduction was 16 ppm at 200 °C and increased to 93 ppm at 300 °C. Similar to the experiment with 250 ppm NH_3, the decline of NO_x reduction above 300 °C was again because of NH_3 loss by oxidation.

The increase in the NO_2 concentration to 500 ppm at 250 ppm NH_3 led to a further increase in NO_x reduction above 250 °C, with a maximum of 100 ppm NO_x reduction at 300 °C. The flattening of the curve was again a result of the occurrence of NH_3 oxidation, which shows the limitation of the NO_x reduction efficiency based on the amount of NH_3 available under these conditions.

Although we showed that NH_3 could not reduce NO over Printex U, a significant increase in the NO_x reduction was observed when NO was added to a feed gas that contained NO_2 and NH_3 over the whole temperature range (for 250 ppm NO_2 + 250 ppm NH_3 + 250 ppm NO, shown in Figure 4). At 200 °C a NO_x reduction of 60 ppm was reached, which was increased up to 140 ppm at 350 °C. However, the addition of NO to the feed gas did not obviate the decrease in the NO_x reduction at temperatures above 300 °C because of the NH_3 limitation.

The calculation of the reaction stoichiometries is a very simple method to determine the ongoing reactions in a reaction system. In our case, the reaction stoichiometries were calculated via the stoichiometric ratio *A* according to 8, and the results were compared to the stoichiometric ratios of the known SCR reactions 3−5. The trends obtained for different concentrations of NO_2, NO, and NH_3 are plotted as a function of temperature in Figure 5. For 250 ppm NO_2 + 250 ppm NH_3, the stoichiometric ratios of 1.35−1.40 were found at 250−300 °C, whereas the ratio was between 1.28 and 1.33 when the NH_3 feed gas concentration was increased to 500 ppm. At 200 °C, the ratio decreased for 250 ppm NH_3 and also for 500 ppm NH_3. However, at this low temperature, the measurement error was higher because of the small conversion rates. At temperatures above 300 °C, the stoichiometric ratios increased because the unselective NH_3 oxidation became more pronounced in this temperature range. The increase in the NO_2 concentration from 250 ppm to 500 ppm led to stoichiometric ratios of 1.28−1.33 at 200−300 °C. At 350 °C, the ratio increased as a consequence of unselective NH_3 oxidation for all concentrations. The calculated values correspond to the *NO_2 SCR* reaction 5, which features a theoretical stoichiometric ratio of 1.33. As such, the *NO_2 SCR* reaction 5 best describes the overall reaction under these conditions.

Compared to the experiment with 0 ppm NO, the experiment that involved the addition of 100 ppm NO to the feed gas resulted in a significant decrease in the stoichiometric ratio to less than 1.33 at 250 and 300 °C. Furthermore, an increase in the NO concentration to 500 ppm resulted in a further decrease of the stoichiometric ratios to approximately 1. From this observation, we concluded that the reaction on the soot surface was shifted from the *NO_2 SCR* reaction in the absence of NO to the *fast SCR* reaction by the addition of NO, according to reaction 4. In the experiment with an NO dosage of 100 ppm, the stoichiometric ratios most likely indicate the occurrence of the *fast SCR* in parallel with the *NO_2 SCR* reaction. An increase in the NO concentration shifted the reaction regime more and more to the *fast SCR* reaction and resulted almost exclusively in the *fast SCR* reaction for 250 ppm NO_2 + 250 ppm NO.

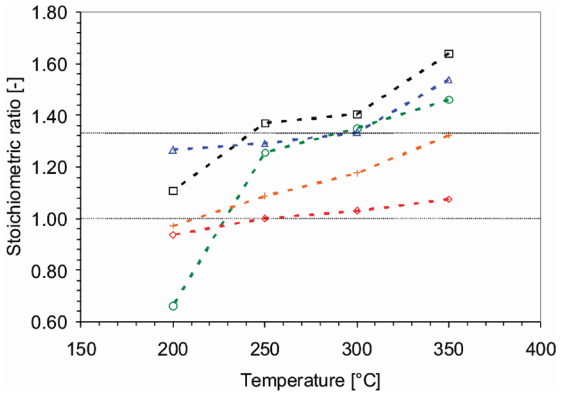

Figure 5. Dependence of the measured stoichiometric ratios over Printex U of the NO_2, NO and NH_3 concentrations between 200 and 350 °C. Black open squares, 250 ppm NO_2 + 250 ppm NH_3; green open circles, 250 ppm NO_2 + 500 ppm NH_3; blue open triangles, 500 ppm NO_2 + 250 ppm NH_3; orange plus signs, 250 ppm NO_2 + 250 ppm NH_3 + 100 ppm NO; red open diamonds, 250 ppm NO_2 + 250 ppm NH_3 + 250 ppm NO. The dotted lines parallel to the *x*-axis highlight the stoichiometries of the *fast SCR* and *NO_2 SCR* reaction calculated from the overall SCR reactions 3 and 4. In comparison to Figure 4 the experiment with 100 ppm NO was added to show the shift from the *NO_2 SCR* reaction regime to the *fast SCR* regime with increasing NO concentration.

3.4. C-Oxidation Rates of Printex U in the Presence of NO_2, NO, and NH_3. In the presence of NO_x, NH_3, and O_2 on soot, not only the SCR reaction occurs, but also the oxidation of soot to CO and CO_2 has to be considered. It was, therefore, important to investigate the influence of different SCR conditions on the parallel-occurring soot oxidation.

In general, soot oxidation can be described in three steps, which are independent of the oxidant. First, an oxidant molecule adsorbs on the soot surface. In the second step, the oxidant transfers an oxygen atom to the surface, forming an oxygen−carbon complex. In the last step this complex decomposes under formation of CO_2 or CO.

Under SCR conditions O_2 and NO_2 are potential species for soot oxidation, while NO_2 exhibits a higher reactivity for soot oxidation at low temperatures. In the literature three mechanisms for soot oxidation in the presence of both O_2 and NO_2 are proposed, which are strongly dependent on soot structure and origin: Messerer et al. proposed a parallel noninterfering mechanism of O_2 and NO_2 with active sites on the soot surface leading to the formation of oxygen surface functional groups.[28] These surface functional groups decompose directly or after further oxidation by one of the oxidant molecules into CO and CO_2. On the other hand, Setibudi et al. and Jaquot et al. presented a co-operative mechanism, where NO_2 reacts with active carbon sites forming oxygen containing-surface functional groups under evolution of NO. These functional groups react with O_2 or NO_2 evolving CO_2, CO and in the case of NO_2 also NO.[24,29] The active carbon sites were

dx.doi.org/10.1021/cs300184q | *ACS Catal.* 2012, 2, 1507−1518

assumed to be unreactive for O_2 before the first NO_2 attack, but after their oxidation with NO_2 they are active for an O_2 attack. A second co-operative mechanism was proposed by Jeguirim et al. However, these authors assumed that O_2 adsorbs first on the soot surface and forms carbon−oxygen complexes, which are attacked faster by NO_2 than O_2 evolving NO, CO and CO_2.[30]

In Figure 6, the overall C-oxidation rates at different NH_3, NO_2, and NO concentrations at 250 °C are plotted along with the NO_2 consumption in ppm.

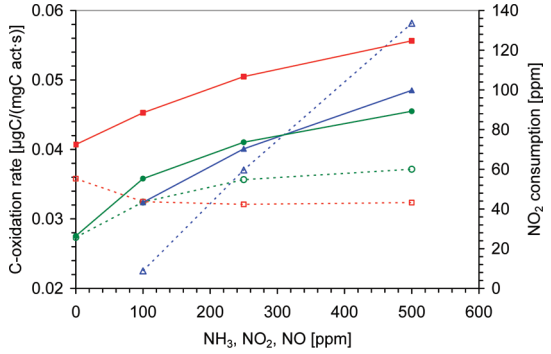

Figure 6. Dependence of the C-oxidation rates and the NO_2 consumption of Printex U during the SCR activity measurements on the NH_3, NO_2, and NO concentrations at 250 °C. Concentrations in the base feed gas: green open and filled circles, 250 ppm NO_2 + variable NH_3 concentrations; blue open and filled triangles, 250 ppm NH_3 + variable NO_2 concentrations; red open and filled squares, 250 ppm NO_2 + 250 ppm NH_3 + variable NO concentrations. Dotted lines and open symbols refer to the C-oxidation rate; solid lines and closed symbols refer to the NO_2 consumption.

The comparison of the C-oxidation rates for different NH_3 concentrations showed that the rates at 0 ppm and 100 ppm NH_3 were slightly lower than those at 250 ppm and 500 ppm NH_3, which was also the case at 200 °C (results not shown) most probably because of an increased formation of by-products. The NO_2 concentration decreased with increasing NH_3 concentration from 0 to 500 ppm NH_3 because of its consumption in the SCR reaction. At temperatures above 300 °C (results not shown), the inverse situation was observed for the C-oxidation rates: In the absence of NH_3 they were highest and decreased with increasing NH_3 concentration since NO_2 was consumed more rapidly at higher temperatures by the SCR reaction and was no longer available for soot oxidation. This was also confirmed by the NO_2 consumption, which increased although the C-oxidation rate decreased.

Variation in the NO concentration showed that, without NO, the C-oxidation rate slightly exceeded the values obtained in the experiments with NO in the feed gas, while the NO_2 consumption increased significantly with the amount of NO. For 100 ppm NO, the C-oxidation rates were still slightly higher than those for 250 ppm and 500 ppm NO because the increased NO_2 consumption by SCR in the presence of NO led to smaller amounts of NO_2 being available for soot oxidation. This trend was also observed at 200 and 300 °C; however, at temperatures above 300 °C, the C-oxidation rates in the absence of NO were less than those observed when NO was included in the reactive gas. This result was most likely because in the presence of NO, a smaller amount of the carbon sample was consumed by oxidation with NO_2 between 250 and 300 °C, which then resulted in the higher C-oxidation rates observed at 350 °C.

The C-oxidation rates for different NO_2 feed gas concentrations showed that an increase in the NO_2 concentration led to an expected increase in the C-oxidation rate. In addition, also the absolute NO_2 consumption increased because of an increased consumption by C-oxidation and SCR reaction (see also Figure 4). With increasing temperature, the C-oxidation rates increased; however, their relative positions were maintained.

The obtained C-oxidation rates with different NH_3, NO and NO_2 concentrations showed that the influence of the SCR conditions on soot oxidation was relatively weak. This result suggested that nitrogen species involved in the SCR process did not affect the decomposition of the surface functional groups responsible for the soot oxidation, irrespective of whether they are chemisorbed or physisorbed.

3.5. Byproducts Generated in the Presence of NO_2, NO, and NH_3 over Printex U. In all experiments, HCN, HNCO, N_2O, HNO_3, and HONO concentrations were also recorded because they are potential reaction intermediates in the SCR reaction and soot oxidation or potential products of unselective side reactions. It seemed that these species were the only byproducts in detectable amounts, since other IR-active byproducts were not found in the spectra. This was supported by the fact that the amount of nitrogen added to the feed gas as NO_x and NH_3 was the same as the sum of nitrogen from NO_x, NH_3, HCN, HNCO, N_2O, HNO_3, and HONO downstream of the reactor plus the amount of NO_x and NH_3 removed by SCR. In Figure 7 and Figure 8, the concentrations of HCN, HNCO,

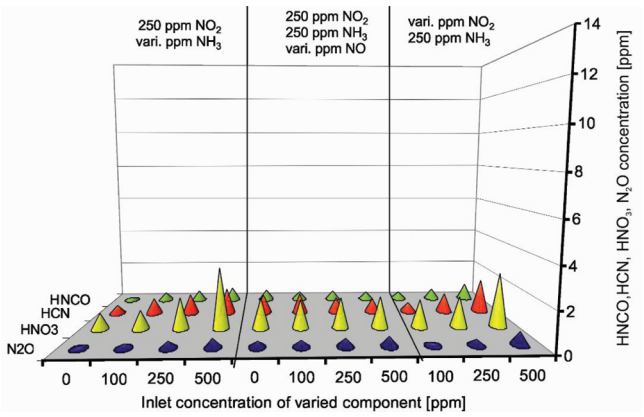

Figure 7. Dependence of the byproducts of the SCR reaction on Printex U on the NH_3, NO_2, and NO concentrations at 200 °C.

N_2O, and HNO_3 are shown for the SCR measurements with different NO_2, NH_3, and NO concentrations at 200 and 350 °C, respectively. HONO was not included in the graphs because it showed a distinct cross-sensitivity with NH_3 in the FTIR analysis and a background shift over the duration of the experiment. However, at the beginning of the measurements after the addition of 250 ppm NO_2 but before the NH_3 dosage, up to 5 ppm HONO was evolved. Therefore, HONO is reasonably assumed to have also formed in the presence of NH_3, although we could not measure it. The HNO_3 concentrations have to be interpreted carefully because they were also slightly cross-sensitive with NH_3.

NH_3 Variation (Figure 7 and Figure 8 - Left Segments). When 250 ppm NO_2 were dosed to the base feed gas in the absence of NH_3, small amounts of HCN and HNCO were found in the absence of NH_3, whereas N_2O and HNO_3 barely

dx.doi.org/10.1021/cs300184q | ACS Catal. 2012, 2, 1507−1518

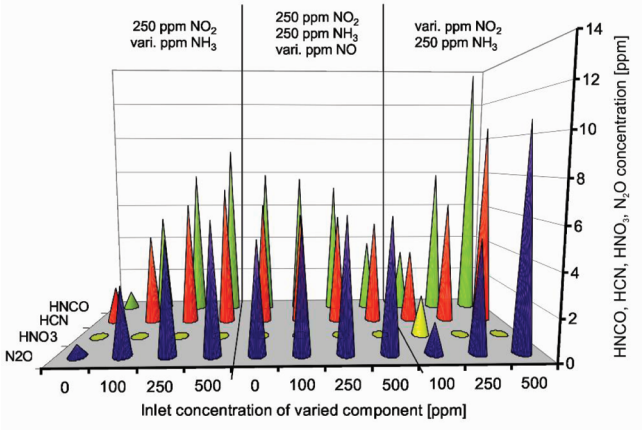

Figure 8. Dependence of byproducts of the SCR reaction on Printex U on the variable NH_3, NO_2, and NO concentrations at 350 °C.

exceeded their detection limits at 200 °C (Figure 7 − left segment). By adding 100 ppm NH_3, the side-product formation slightly increased, which could be enforced by increasing the NH_3 concentration to 250 ppm and even more for 500 ppm. HCN, HNCO, and N_2O exhibited a significant increase in concentration with increasing temperature, as evident from a comparison of the results for the different NH_3 concentrations at 200 °C (Figure 7 − left segment) and 350 °C (Figure 8 − left segment). The large amounts of HCN and HNCO observed under these conditions also explain the slightly increased C-oxidation rates observed when 250 and 500 ppm NH_3 were dosed (see section 4.4).

HNO_3 showed a different behavior compared to the other components. At 200 °C, the concentration of HNO_3 increased with increasing NH_3 concentration; however, with increasing temperature, the concentration of HNO_3 in the outlet gas flow decreased and reached its detection limit at 350 °C, independent of the NH_3 concentration. This might be construed as a reduced HNO_3 formation on the soot surface at higher temperatures, but it is more likely that the reaction rate of HNO_3 was larger than the rate of desorption leading to a reduced concentration in the outlet gas flow.

NO Variation (Figure 7 and Figure 8 - Middle Segments). In the middle of Figure 7 and Figure 8 the amounts of emitted byproducts for different amounts of NO at constant NO_2 and NH_3 concentrations (both 250 ppm) are shown. At 200 °C, small amounts of HNO_3 were emitted, and these amounts were not influenced by the NO variation or by temperature up to 300 °C (results not shown). However, at 350 °C, no HNO_3 was detected because the rate of desorption was again smaller than the rate of reaction (Figure 8) as already described for the NH_3 variation in the previous section. N_2O showed an increase with increasing temperature but was rather independent of the NO concentration especially at 350 °C. The HCN and HNCO concentrations increased with increasing temperature; interestingly, however, HCN and, to a greater extent, HNCO decreased with increasing NO concentration.

NO_2 Variation (Figure 7 and Figure 8 - Right Segments). On the right sides of Figure 7 and Figure 8, the results of the HCN, HNCO, and N_2O measurements at different NO_2 concentrations but constant NH_3 concentration (250 ppm) are presented. Similar to the variation of NH_3, increasing temperature and NO_2 concentration resulted in greater amounts of HCN, HNCO, and N_2O. HNO_3, however, again exceeded its detection limit only at 200 °C because of the higher rate of reaction in comparison to the rate of desorption. With 500 ppm NO_2 and 250 ppm NH_3, concentrations as high as 10 ppm HCN, 14 ppm HNCO, and 10 ppm N_2O were observed at 350 °C. These values were the highest observed concentrations throughout the experimental series.

Formation Mechanisms of Byproducts. In the following, the formation pathways of the HCN, HNCO, N_2O, HNO_3, and HONO will be presented. They are mostly based on reactions known in organic chemistry and are able to explain the ongoing reactions under SCR conditions.

HCN was most probably formed from the decomposition of surface nitriles, which resulted from a reaction between NH_3 and carboxylic surface functional groups as shown in Figure 9.

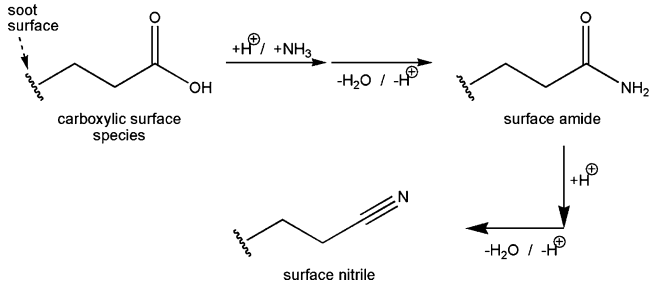

Figure 9. Formation of surface nitriles from the reaction between NH_3 and carboxylic surface species. The α-carbon atom might be either saturated by hydrogen, alkyl species, or hetero atomic groups (e.g., hydroxylic group).

In the first step, NH_3 reacted with a carboxylic group, forming a surface amide, which decomposed in a second step similar to the back reaction of liquid-phase nitrile hydrolysis into the surface nitrile:[31]

These nitrile groups were indicated by C═N vibrations that were observed in the region between 1700 and 1500 cm^{-1} in the DRIFTS measurements during this study; they were also confirmed by Zawadzki et al.[27] Additionally, we also found absorption bands of acidic groups during the DRIFTS measurements in the 1700−1500 cm^{-1} (C═O) region and at 1310−1100 cm^{-1} (C−O), as was also previously reported.[22,32] The assumption of a reaction between NH_3 and carboxylic surface species was supported by two facts: First, the gas phase concentrations of HCN and also HNCO decreased when the NO concentration was increased (Figure 7 and Figure 8 − middle). This was due to an acceleration of the SCR reaction by NO, which led to a limitation of the amount of NH_3 available for side reactions. (A decrease of HCN and HNCO because of a redox reaction with NO leading to N_2 and CO or CO_2, respectively, could be excluded after an analysis of the oxidation numbers of the involved species.) And second, the amounts of emitted HCN and HNCO increased with increasing NO_2 and NH_3 concentration. In the case of NO_2 variation, this was most probably due to the pronounced capability of NO_2 to form acidic functional groups on the soot surface.[22] In the case of NH_3, however, the increasing amounts of HCN and HNCO were not due to the formation of these acidic functional groups, but to an increase of the amount of NH_3 available for the reaction with previously formed acidic functional groups.

For the decomposition of the surface nitriles under evolution of HCN, two reactions are plausible: The first possibility is the decomposition of the nitrile into an alkene and HCN, similar to

dx.doi.org/10.1021/cs300184q | ACS Catal. 2012, 2, 1507−1518

the back reaction of hydrocyanation.[33,34] The second possibility, in the case of surface hydroxyl nitrile species, is the decomposition into HCN and a carbonyl species,[35] as shown in Figure 10.

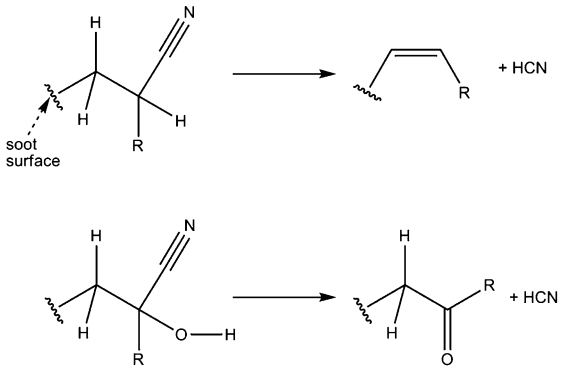

Figure 10. Decomposition of surface nitriles formed as shown in Figure 9 into HCN and a surface-bound alkene or a surface carbonyl species. R stands for an alkyl species.

We assumed that HNCO was formed by the decomposition of surface isocyanates, which were observed in the DRIFTS spectra. We observed a peak with a maximum at 2208 cm^{-1}, which was attributed to isocyanate species.[27,36] These surface isocyanates most likely also originate from surface amides similar to the surface nitriles in Figure 9. However, in this case a rearrangement of the surface amides is responsible for the formation of the surface isocyanates. This rearrangement on the soot surface might proceed via intermediates similar to those of the Hofmann rearrangement of isolated molecules in the liquid phase,[31,35] as schematically depicted in Figure 11. Because

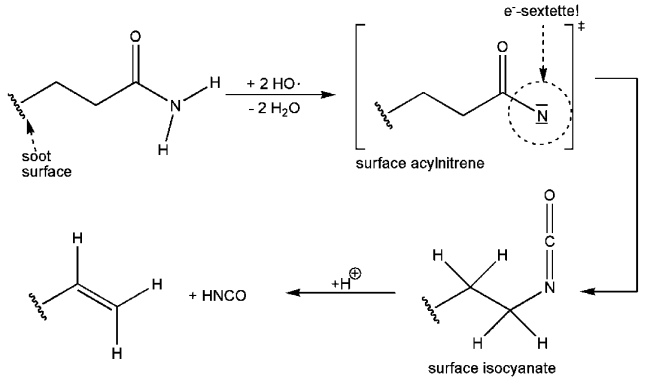

Figure 11. HNCO formation from the decomposition of surface amides.

hypobromite, which is used as base for the classical Hofmann rearrangement, is missing over soot, we suggest that OH· radicals formed during soot oxidation assume the role of the base for acylnitrene formation. Because the acylnitrene has only an electron sextet, it stabilizes itself through rearrangement to an isocyanate, which was assumed to decompose under the formation of HNCO and an alkene in the last step.

N_2O resulted from a comproportionation reaction during NO_x reduction, which can be formally described by eq 10 or from the oxidation of NH_3 (eq 11).[5] Therefore, it was expected to increase with the NH_3 and NO_2 concentration as well as with temperature. This expected result was confirmed by the trends presented in Figure 7 and Figure 8. In section 4, it will be shown that eq 10 is the summary of several reaction steps, which are directly involved in the NO_x reduction; however, here we use the overall equation to simplify matters.

$$2NH_3 + 2NO_2 \rightarrow N_2O + N_2 + 3H_2O \quad (10)$$

$$3NH_3 + 4NO_2 \rightarrow 3.5N_2O + 4.5H_2O \quad (11)$$

HNO_3 and HONO are known to be formed in the presence of water even at room temperature (RT) on the soot surface by a disproportionation of NO_2 (eq 12).[37−39] The detection of HNO_3 and HONO during the experiments without NH_3 in the feed gas suggests that this reaction also occurs under the reaction conditions used in our study:

$$2NO_2 + H_2O \rightarrow HONO + HNO_3 \quad (12)$$

Furthermore, HONO could be generated via hydrogen abstraction from the soot surface by NO_2, as has been shown in ref.[40] and is known to occur during the partial oxidation of light organic molecules in the gas phase.[41]

3.6. SCR Activity of Diesel Soot. After the SCR activity of the synthetic soot Printex U was investigated, selected experiments were performed with the real diesel soot (Euro V, Euro 0, and mixed soot) samples to probe the dependence of their NO_x reduction ability at 250 and 300 °C on the NO, NO_2, and NH_3 concentrations. At 300 °C (Figure 12), the mixed

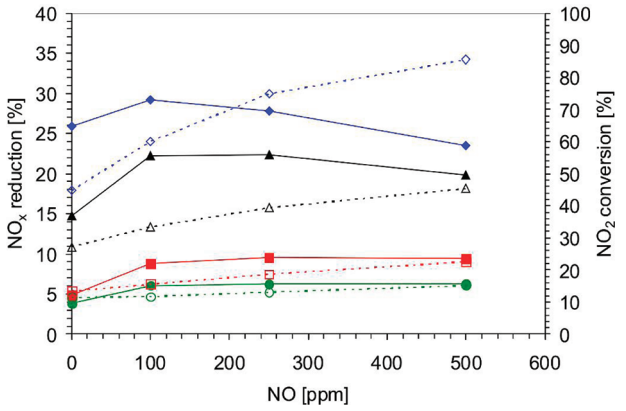

Figure 12. Dependence of the NO_x reduction and NO_2 conversion over Euro 0 soot, Euro V soot, and the mixed soot sample on the NO concentration at 300 °C compared to Printex U. Concentrations in the basic feed gas: 250 ppm NO_2 + 250 ppm NH_3 + variable NO concentrations. Blue filled and open diamonds, Printex U; black filled and open triangles, mixed soot; red filled and open squares, Euro V; green filled and open circles, Euro 0. Solid lines and closed symbols: NO_x reduction; dotted lines and open symbols: NO_2 conversion.

soot sample showed a NO_x reduction of approximately 14% in the presence of 250 ppm NO_2 + 250 ppm NH_3, which is 55% of the NO_x reduction obtained for Printex U. With a rate of approximately 5%, the Euro 0 and Euro V soots were only slightly active for NO_x reduction at 0 ppm NO. The addition of 100 ppm NO enhanced the rates for all samples.

Similar to the experiments with Printex U, stoichiometric ratios of approximately 1 were measured in the presence of NO, which indicated the *fast SCR* reaction. In the absence of NO, the stoichiometric ratios increased to 1.4 for all samples, which indicated the *NO_2 SCR* reaction. Higher amounts of NO led to a decrease in the NO_x reduction for the mixed soot sample and for Printex U, which may appear to indicate a

dx.doi.org/10.1021/cs300184q | ACS Catal. 2012, 2, 1507−1518

decreased SCR activity. However, the NO_2 conversion plotted on the secondary *y*-axis in Figure 12 increased, which showed that the decrease in the NO_x reduction was not due to a loss of activity. In fact, this result was due to the limited amount of available NO_2 and the fact that NO could not be reduced by NH_3 in the *standard SCR* reaction in the absence of NO_2 (Figure 3). Apparently, the rates of Euro 0 and Euro V remained constant at approximately 5% in the range of the experimental error, even after the addition of 250 ppm and 500 ppm NO. However, because of the low overall conversion, small changes in the NO_x reduction rates in the presence of excess NO might not be resolved.

As expected, at 250 °C, NO_x reduction decreased for all of the samples, which led to a rate of approximately 9% for the mixed soot, which is almost two-thirds the rate of Printex U. The rate of less than 3% for the Euro 0 and Euro V soots indicated that they were minimally active for NO_x reduction under these conditions. Again, the addition of 100 ppm NO enhanced the rates for all of the samples. Higher amounts of NO led to decreased NO_x reduction for the mixed soot sample because excess NO could not be removed, as previously discussed for the experiments conducted at 300 °C.

The trends observed for the variation of the NO_2 and NH_3 concentrations at 250 and 300 °C for the real diesel soot samples were similar to those obtained for Printex U; with increasing NH_3 concentration, the NO_x reduction also increased, whereas the NO_x reduction decreased with increasing NO_2 concentration because of the constant NH_3 concentration. In addition, the order of the soot samples observed for the NO variation was similar, independent of the NO_2 and NH_3 concentration; Printex U was the most active, followed by the mixed soot sample, whereas the Euro V and Euro 0 showed the lowest activity in the series.

In Figure 13, the byproducts generated during the SCR measurements at 250 and 300 °C with 250 ppm NO_2 and 250 ppm NH_3 for the three diesel soot samples are shown compared to Printex U. The data clearly demonstrate that with increasing activity of the soot samples, greater amounts of N_2O, HCN, and HNCO were evolved, whereas less active samples evolved more HNO_3. The observed relative trends between the four soot samples were the same for other concentrations of NO_2 and NH_3 as well as in the presence of NO.

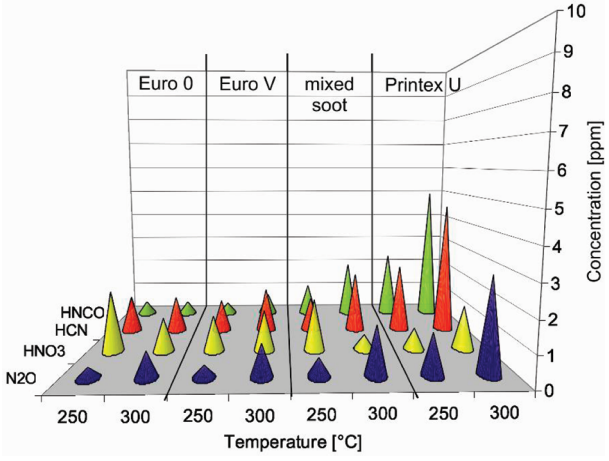

Figure 13. Dependence of the byproducts of the SCR reaction on Printex U, Euro 0 soot, Euro V soot, and the mixed soot sample on the NH_3 at 250 and 300 °C at a GHSV of 35,000 h^{-1}. Concentrations in the basic feed gas: 250 ppm NO_2 + 250 ppm NH_3.

The C-oxidation rates of the mixed soot sample were barely influenced by changes in the NH_3 and NO concentrations. The C-oxidation rates of the Euro V and Euro 0 samples, which were lower than the rates of the mixed soot sample independent of the gas composition, were also not influenced by variation of the NH_3 concentration. In contrast, the variation of NO led to a small decrease in C-oxidation because more NO_2 was consumed in the SCR process. An increase in the NO_2 concentration led to the expected corresponding increase in the C-oxidation rates for the diesel soot samples. However, the measured C-oxidation rates of the diesel soot samples were significantly lower than those obtained for Printex U at 250 °C, and this difference was even more pronounced at 300 °C.

In the following section, the reasons that could explain the differences between the four soot samples will be discussed. In the literature, different activated carbon materials with different activities for NO_x removal have been described;[11,12,18,20,42−48] however, the reasons for their activity could not be definitively clarified. At a minimum, the occurrence of acidic surface functional groups for NH_3 adsorption was identified as an important property of an SCR-active carbon material.[20,49−52] The authors reported that measures that increased the number of acidic groups also resulted in an increase in the SCR activity. From investigations of the soot oxidation in the presence of NO_2,[22] we concluded that NO_2 promotes the formation of surface carboxylic acids and lactones differently on the four soot samples used for this study. Therefore, Printex U most likely exhibited the highest activity in the series toward the formation of acidic surface functional groups on the carbon surface, which led to an increased NH_3 adsorption. This assumption was also supported by the higher amounts of evolved HCN and HNCO (Figure 13) and the increased C-oxidation rates found for Printex U and, to a lesser extent, for mixed soot because acidic surface functional groups decompose at lower temperatures compared to more basic groups.[22]

In addition to the influence of the surface functional groups, alkali metals found in the ashes of the diesel soot samples might also contribute to the lower SCR activity compared to that of Printex U (Table 2). These metals are strongly basic, and Ahmed et al. have reported that they inhibit the SCR activity of activated carbons for NO_x removal.[53] However, this hypothesis was not investigated in more detail in the present work.

As already reported by other authors,[50,53] the BET surface area did not appear to influence the SCR activity because Printex U showed the highest activity despite exhibiting the lowest surface area.

3.7. SCR Effect over Diesel Soot in the Presence of H_2SO_4. The higher NO_x reduction activity of the mixed soot sample compared to those of the Euro V and Euro 0 soots was explained by an increased ability of the mixed soot to form acidic surface functional groups. However, the presence of H_2SO_4 (2.3 wt % − Figure 2), which was observed during the compositional analysis of the mixed soot sample as SO_2, might also contribute to the higher activity. In the literature, the activity of carbon materials for NO_x reduction were reported to be increased by impregnation with H_2SO_4 followed by calcination.[18] Again, this enhancement was explained by the increase in the number of acidic surface groups due to the oxidative nature of H_2SO_4. In the mixed soot sample, a similar mechanism is conceivable because the H_2SO_4 might have oxidized the surface during heating to the reaction temperature;

dx.doi.org/10.1021/cs300184q | *ACS Catal.* 2012, 2, 1507−1518

however, a direct influence of H_2SO_4 on the NO_x reduction also appeared to be possible. To investigate this hypothesis, isothermal NO_x reduction experiments were performed at 200 and 250 °C with Printex U-coated monoliths impregnated with H_2SO_4. The NO_2, NO, and NH_3 concentrations were varied according to Table 1. The results of the NH_3 variation are shown in Figure 14. Independent of the NH_3 concentration and

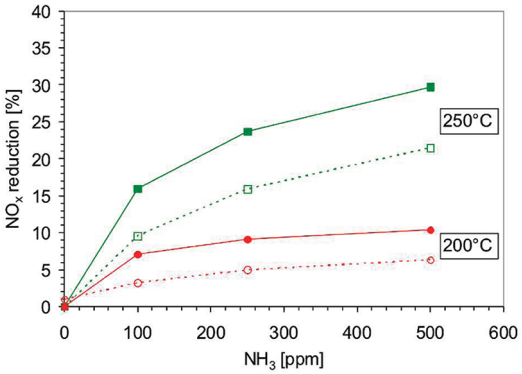

Figure 14. NO_x reduction over Printex U impregnated with 5 mg of sulfuric acid at 200 °C (red filled and open circles,) and 250 °C (green filled and open squares) as a function of the NH_3 concentration. The results for Printex U without impregnation are included for comparison. Concentrations in the basic feed gas: 250 ppm NO_2 and variable NH_3 concentrations. Dotted line and open symbols: without H_2SO_4; solid lines and filled symbols: with H_2SO_4.

independent of the temperature, the NO_x reduction was significantly increased in the presence of H_2SO_4. Similar results were also observed for the experiments in which NO and NO_2 were varied. The concentrations of the measured byproducts were similar to those determined in the experiments conducted without H_2SO_4.

The results supported the hypothesis of a direct influence of H_2SO_4 on the NO_x reduction activity, which was most likely not due to the formation of more acidic surface functional groups.

4. MECHANISM

Before the mechanism of NO_x reduction, which was developed based on the experimental data, is described, the most important results and conclusions should be summarized: First, we observed minimal coupling of the C-oxidation rates and the SCR reaction. Therefore, we concluded that the NO_x involved in the SCR reaction on soot did not form strong bonds with the soot (e.g., surface nitrates and nitrites) and had a more physisorbed nature. This result also indicates that the HNCO and HCN found in the gas phase and the C−N and C−O bonds of surface species observed in the DRIFTS measurements did not take part in the SCR process and were only involved in the soot oxidation. The adsorption of NH_3, however, is most likely supported by the presence of acidic surface functional groups because of the acid−base interactions.[20,45,48,49,54,55] The resulting ammonium ions (NH_4^+) act as counterions for the acidic surface functional groups; however, the ammonium ions did not seem to influence the decarboxylation of these groups during soot oxidation. Second, stoichiometries were measured, which imply that the *NO_2 SCR* (5) reaction is dominant in the absence of NO and that the *fast SCR* reaction 4 is dominant in the presence of NO. The *standard SCR* reaction 3 was excluded because of the SCR inactivity of soot in the absence of NO_2. Third, HONO and HNO_3 were formed as byproducts, which was taken as confirmation of the heterogeneous disproportionation of NO_2 on the soot surface.

The heterogeneous disproportionation of two NO_2 molecules into HONO and HNO_3 (eq 12) is likely the initial step of the NO_x reduction over soot. This step has not only been discussed in relation to the *NO_2 SCR* (eq 5) and *fast SCR* (eq 4) reactions on inorganic catalysts in the presence of H_2O[56] but has also been observed on other surfaces (e.g., soot and SiO_2 particles) at RT during investigations related to atmospheric chemistry.[38,39,57] This disproportionation reaction was confirmed in this study by the evolution of HONO and HNO_3 during the measurements:

$$2NO_2 + H_2O \rightarrow HONO + HNO_3 \quad (12)$$

This disproportionation was likely also the step that was promoted by H_2SO_4 that led to the higher NO_x reduction evident in Figure 14. We assumed that this promotion by H_2SO_4 was due to the protonation of N_2O_4, which facilitated the attack of water. The presence of H_2SO_4 might also explain the higher NO_x reduction ability of the mixed soot sample compared to the Euro 0 and Euro V samples because the composition analysis of the mixed soot showed that it contained up to 2.3% H_2SO_4.

HONO and HNO_3 are assumed to remain physisorbed on the surface, where they form ammonium nitrate (NH_4NO_3) and ammonium nitrite (NH_4NO_2) in the presence of NH_3:[56]

$$2NH_3 + HONO + HNO_3 \rightarrow NH_4NO_2 + NH_4NO_3 \quad (13)$$

The NH_4NO_2 and NH_4NO_3 in 13 should be considered as isolated molecules or ionic species at the soot surface and not bulk material. It is important to note that the occurring chemistry is described formally and could also be described using an ionic formulation.

After the formation of the nitrite, it decomposes immediately into nitrogen and water and thereby forms the first nitrogen molecule[6] because NH_4NO_2 is unstable at temperatures above 60 °C:[58]

$$NH_4NO_2 \rightarrow N_2 + H_2O \quad (14)$$

The remaining NH_4NO_3 decomposes again into HNO_3 and NH_3:[59]

$$NH_4NO_3 \rightarrow HNO_3 + NH_3 \quad (15)$$

In the *fast SCR* mechanism, which occurred in the presence of NO, as confirmed by the stoichiometric ratios found in this study, the HNO_3 is reduced by NO in a subsequent step:[60]

$$HNO_3 + NO \rightarrow NO_2 + HONO \quad (16)$$

The formed HONO again reacts with NH_3 to form NH_4NO_2 according to eq 13, which then decomposes to nitrogen and water, eq 14. The summation of reactions 12 and 13−15 leads to the overall equation for the *fast SCR* reaction, eq 4.

The stoichiometry of the *NO_2 SCR* mechanism was observed during the measurements conducted without NO in the feed gas. In this mechanism, the reactions are similar to the *fast SCR* mechanism up to eq 15, but eq 16 does not occur because NO is missing as the reducing agent. According to the observed stoichiometric ratio, NH_3 serves as the reducing agent for NH_4NO_3 in the case of the *NO_2 SCR* reaction:[59]

dx.doi.org/10.1021/cs300184q | *ACS Catal.* 2012, 2, 1507−1518

$$3NH_4NO_3 + 2NH_3 \rightarrow 4N_2 + 9H_2O \quad (17)$$

The summation of reactions 12, 13−15 and 17 leads to the known overall *NO_2 SCR* reaction 5.

The consumption of HNO_3 according to reactions 16 and 17 during the SCR process on soot was supported by the comparison of the diesel soot samples and Printex U. The diesel soot samples with a lower SCR activity evolved greater amounts of HNO_3 because it was not consumed in the further SCR process. Therefore, a mechanism that excludes NH_4NO_3, such as that proposed by Richter et al. and Jüntgen et al.,[14,15] can probably be excluded for the soot samples used in the present study. Furthermore, the observed HNO_3 emissions led to the conclusion that the disproportionation step 12 does not limit the SCR reaction and that the presence of adsorption sites for NH_3 is likely the limiting factor. The SCR chemistry on the soot surface is summarized schematically in Figure 15.

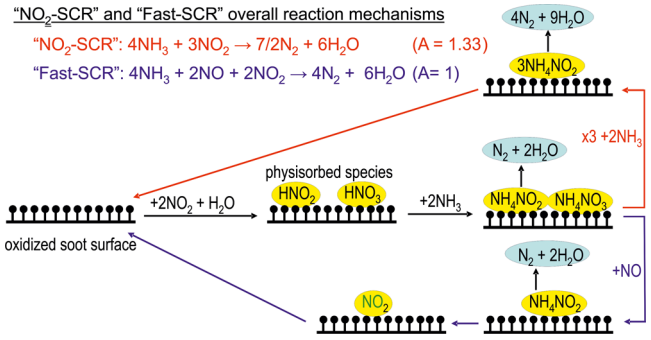

Figure 15. Suggested mechanism for the selective catalytic reduction of NO_x on diesel soot. The dark points symbolize acidic carbon surface species supporting NH_3 adsorption.

For the sake of completeness, the byproducts produced during the SCR investigations, in addition to HONO and HNO_3, will be discussed, although, they were previously discussed in section 4.5. N_2O was formed according to reaction 18 from the decomposition of NH_4NO_3 at temperatures above 200 °C,[59] which is one part of reaction 10, while the second part of reaction 10 is the formation and decomposition of NH_4NO_2 leading to nitrogen and water.

$$NH_4NO_3 \rightarrow N_2O + 2H_2O \quad (18)$$

Another pathway for the formation of N_2O is the oxidation of NH_3 with NO_2 according to reaction 10.[56] Although HCN and HNCO were formed from the reaction of carboxylic functional groups with NH_3, as indicated by the DRIFTS investigations, both species did not contribute to the NO_x reduction.

5. CONCLUSIONS

The investigations of the reduction of NO_x by the SCR reaction with NH_3 showed that model and diesel soot samples were able to remove NO_x in model exhaust gases up to 25% at 35,000 h^{-1}. The disproportionation of NO_2 is the initial step of the SCR process on soot. Therefore, the presence of NO_2 in the feed gas was a prerequisite because the oxidation of NO was kinetically inhibited because of the high space velocities.

However, when both NO and NO_2 were present in the feed gas, the SCR activity was higher than that measured in the absence of NO because the *fast SCR* reaction proceeded. In the absence of NO in the feed gas, the *NO_2 SCR* reaction pathway was followed. The presence of alkali metals might inhibit the SCR activity.

One may argue that soot cannot be regarded as catalyst in our study because it is consumed during the reaction. However, the consumption of the soot catalyst is due to the oxidation of soot by oxygen and NO_2, which was shown by us to be independent of the SCR reaction. Therefore, the oxidation of soot can be discussed separately from the SCR reaction. Considering the effect of soot on the SCR reaction itself, we did not observe any SCR activity in a blank experiment with uncoated cordierites but in the presence of soot a SCR effect was observed, that is, soot has to be regarded as catalyst for this specific reaction. Since the *fast* and the *NO_2 SCR* reaction do not require a redox-active component, the catalytic function of soot is to provide adsorption sites for ammonia as well as NO_x species.

We believe that the observed SCR effect on diesel soot can be exploited to improve future diesel exhaust aftertreatment systems, where both DPF and SCR systems have to be used in series to reach the desired emission limits. Current research activities are aimed at the combination of both aftertreatment systems into a single device, for example, in the form of an SCR-coated DPF, to reduce size and weight. Such a combined system requires urea dosage upstream of the SCR-DPF device. Because NO_2 is usually produced from NO in a diesel oxidation catalyst to facilitate regeneration of the DPF and to promote the SCR reaction, the relevance of the present study becomes apparent. The observed SCR activity of diesel soot might allow a reduction of the amount of SCR catalyst on such a SCR-coated DPF. However, further investigations are necessary to determine whether the SCR activity of soot is as high in the presence of an SCR catalyst as in the absence of a catalyst.

AUTHOR INFORMATION

Corresponding Author

*E-mail: oliver.kroecher@psi.ch.

Funding

We thank the Swiss National Fund for financial support (Project # 200021_125257).

Notes

The authors declare no competing financial interest.

ACKNOWLEDGMENTS

We thank Dr. D. Rothe (MAN) for providing the diesel soot samples.

REFERENCES

(1) Neeft, J. P. A.; Makkee, M.; Moulijn, J. A. *Fuel Process. Technol.* **1996**, *47* (1), 1−69.
(2) Twigg, M. V. *Appl. Catal., B* **2007**, *70* (1−4), 2−15.
(3) Stanmore, B. R.; Brilhac, J. F.; Gilot, P. *Carbon* **2001**, *39* (15), 2247−2268.
(4) Koebel, M.; Elsener, M.; Kleemann, M. *Catal. Today* **2000**, *59* (3−4), 335−345.
(5) Kröcher, O.; Devadas, M.; Elsener, M.; Wokaun, A.; Soger, N.; Pfeifer, M.; Demel, Y.; Mussmann, L. *Appl. Catal., B* **2006**, *66* (3−4), 208−216.
(6) Yeom, Y. H.; Henao, J.; Li, M. J.; Sachtler, W. M. H.; Weitz, E. *J. Catal.* **2005**, *231* (1), 181−193.
(7) Colombo, M.; Nova, I.; Tronconi, E. *Catal. Today* **2010**, *151* (3−4), 223−230.
(8) Grossale, A.; Nova, I.; Tronconi, E. *Catal. Today* **2008**, *136* (1−2), 18−27.

(9) Lietti, L.; Nova, I.; Ramis, G.; Dall'Acqua, L.; Busca, G.; Giamello, E.; Forzatti, P.; Bregani, F. *J. Catal.* **1999**, *187* (2), 419−435.
(10) Koebel, M.; Elsener, M.; Madia, G. *SAE Technical Paper Series.* **2001**, *SAE 2001-01-3625*.
(11) Jüntgen, H.; Knoblauch, K.; Richter, E.; Schmidt, H.-J.; Folz, M. 1980, DE 2911712.
(12) Jüntgen, H.; Richter, E.; Knoblauch, K.; Hoang-Phu, T. *Chem. Eng. Sci.* **1988**, *43* (3), 419−428.
(13) Knoblauch, K.; Richter, E.; Jüntgen, H. *Fuel* **1981**, *60* (9), 832−838.
(14) Richter, E.; Knoblauch, K.; Jüntgen, H. *Gas Sep. Purif.* **1987**, *1* (1), 35−43.
(15) Jüntgen, H. *Erd. Koh. Erdg. Petr. V.* **1986**, *39* (12), 546−551.
(16) Muniz, J.; Marban, G.; Fuertes, A. B. *Appl. Catal., B* **1999**, *23* (1), 25−35.
(17) Shirahama, N.; Mochida, I.; Korai, Y.; Choi, K. H.; Enjoji, T.; Shimohara, T.; Yasutake, A. *Appl. Catal., B* **2005**, *57* (4), 237−245.
(18) Izquierdo, M. T.; Rubio, B.; de Yuso, A. M.; Ballestero, D. *Fuel Process. Technol.* **2011**, *92* (7), 1362−1367.
(19) Jüntgen, H.; Richter, E.; Kuhl, H. *Fuel* **1988**, *67* (6), 775−780.
(20) Ku, B. J.; Lee, J. K.; Park, D.; Rhee, H.-K. *Ind. Eng. Chem. Res.* **1994**, *33* (11), 2868−2874.
(21) Mehring, M. Ph.D. Thesis No. 19993, ETH Zürich, Switzerland, 2011.
(22) Muckenhuber, H.; Grothe, H. *Carbon* **2007**, *45* (2), 321−329.
(23) Neeft, J. P. A.; Nijhuis, T. X.; Smakman, E.; Makkee, M.; Moulijn, J. A. *Fuel* **1997**, *76* (12), 1129−1136.
(24) Setiabudi, A.; Makkee, M.; Moulijn, J. A. *Appl. Catal., B* **2004**, *50* (3), 185−194.
(25) Mehring, M.; Elsener, M.; Kröcher, O. *J. Therm. Anal. Calorim.* **2011**, *105* (2), 545−552.
(26) Mehring, M.; Elsener, M.; Kröcher, O. *MTZ* **2011**, *72* (9), 690−696.
(27) Zawadzki, J.; Wisniewski, M. *Carbon* **2003**, *41* (12), 2257−2267.
(28) Messerer, A.; Niessner, R.; Poschl, U. *Carbon* **2006**, *44* (2), 307−324.
(29) Jacquot, F.; Logie, V.; Brilhac, J. F.; Gilot, P. *Carbon* **2002**, *40* (3), 335−343.
(30) Jeguirim, M.; Tschamber, V.; Brilhac, J. F.; Ehrburger, P. *J. Anal. Appl. Pyrol.* **2004**, *72* (1), 171−181.
(31) Vollhardt, K.; Schore, N. *Organische Chemie*; Wiley VCH: Weinheim, Germany, 2000; Vol. 3.
(32) Dandekar, A.; Baker, R. T. K.; Vannice, M. A. *Carbon* **1998**, *36* (12), 1821−1831.
(33) Keim, W.; Behr, A.; Lühr, H. O.; Weisser, J. *J. Catal.* **1982**, *78* (1), 209−216.
(34) Puentes, E.; Noels, A. F.; Warin, R.; Hubert, A. J.; Teyssié, P.; Waddan, D. Y. *J. Mol. Catal.* **1985**, *31* (2), 183−190.
(35) Brückner, R. *Reaktionsmechanismen*; Springer: Heidelberg, Germany, 2003; Vol. 2.
(36) Matyshak, V. A.; Krylov, O. V. *Today* **1995**, *25* (1), 1−87.
(37) Akimoto, H.; Bandow, H.; Sakamaki, F.; Inoue, G.; Hoshino, M.; Okuda, M. *Environ. Sci. Technol.* **1980**, *14* (2), 172−179.
(38) Kleffmann, J.; Becker, K. H.; Wiesen, P. *Atmos. Environ.* **1998**, *32* (16), 2721−2729.
(39) Sakamaki, F.; Shiro, H.; Akimoto, H. *Int. J. Chem. Kin.* **1980**, *15*, 1013−1029.
(40) Stadler, D.; Rossi, M. J. *Phys. Chem. Chem. Phys.* **2000**, *2* (23), 5420−5429.
(41) Otsuka, K.; Takahashi, R.; Amakawa, K.; Yamanaka, I. *Catal. Today* **1998**, *45* (1−4), 23−28.
(42) Aarna, I.; Suuberg, E. M. *Fuel* **1997**, *76* (6), 475−491.
(43) Izquierdo, M. T.; Rubio, B.; Mayoral, C.; Andrés, J. M. *Fuel* **2003**, *82* (2), 147−151.
(44) Kuhl, H.; Baumann, H.; Juntgen, H.; Ehrburger, P.; Dentzer, J.; Lahaye, J. *Fuel* **1989**, *68* (1), 129−130.
(45) Martin-Martinez, J. M.; Singoredjo, L.; Mittelmeijer-Hazeleger, M.; Kapteijn, F.; Moulijn, J. A. *Carbon* **1994**, *32* (5), 897−904.
(46) Mochida, I.; Kishino, M.; Kawano, S.; Sakanishi, K.; Korai, Y.; Yasutake, A.; Yoshikawa, M. *Fuel* **1998**, *77* (15), 1741−1746.
(47) Richter, E.; Kleinschmidt, R.; Pilarczyk, E.; Knoblauch, K.; Jontgen, H. *Thermochim. Acta* **1985**, *85*, 315−318.
(48) Singoredjo, L.; Kapteijn, F.; Moulijn, J. A.; Martin-Martinez, J.-M.; Boehm, H.-P. *Carbon* **1993**, *31* (1), 213−222.
(49) Ahmed, S. N.; Baldwin, R.; Derbyshire, F.; McEnaney, B.; Stencel, J. *Fuel* **1993**, *72* (3), 287−292.
(50) Izquierdo, M. T.; Rubio, B.; Mayoral, C.; Andrés, J. M. *Appl. Catal., B* **2001**, *33* (4), 315−324.
(51) Komatsubara, Y.; Ida, S.; Fujitsu, H.; Mochida, I. *Fuel* **1984**, *63* (12), 1738−1742.
(52) Mochida, I.; Kawano, S. *Ind. Eng. Chem. Res.* **1991**, *30* (10), 2322−2327.
(53) Ahmed, S. N.; Stencel, J. M.; Derbyshire, F. J.; Baldwin, R. M. *Fuel Process. Technol.* **1993**, *34* (2), 123−136.
(54) Lee, J. K.; Park, T. J.; Park, D.; Park, S. *Ind. Eng. Chem. Res.* **1993**, *32* (9), 1882−1887.
(55) Szymanski, G. S.; Grzybek, T.; Papp, H. *Catal. Today* **2004**, *90* (1−2), 51−59.
(56) Devadas, M.; Kröcher, O.; Elsener, M.; Wokaun, A.; Soger, N.; Pfeifer, M.; Demel, Y.; Mussmann, L. *Appl. Catal., B* **2006**, *67* (3−4), 187−196.
(57) Grassian, V. H. *J. Phys. Chem. A* **2002**, *106* (6), 860−877.
(58) Laue, W.; Thiemann, M.; Scheibler, E.; Wiegand, K. W. Nitrates and Nitrites. In *Ullmann's Encyclopedia of Industrial Chemistry*, Wiley-VCH: Weinheim, Germany, 2012; pp 149−176.
(59) Grossale, A.; Nova, I.; Tronconi, E. *Catal. Lett.* **2009**, *130* (3), 525−531.
(60) Nova, I.; Ciardelli, C.; Tronconi, E.; Chatterjee, D.; Bandl-Konrad, B. *Catal. Today* **2006**, *114* (1), 3−12.